Journal of Biomolecular NMR, **16:** 127–138, 2000.
KLUWER/ESCOM

NMR experiments for resonance assignments of ^{13}C, ^{15}N doubly-labeled flexible polypeptides: Application to the human prion protein hPrP(23–230)

Aizhuo Liu*, Roland Riek, Gerhard Wider, Christine von Schroetter, Ralph Zahn & Kurt Wüthrich**
Institut für Molekularbiologie und Biophysik, Eidgenössische Technische Hochschule Hönggerberg, CH-8093 Zürich, Switzerland

Received 25 September 1999; Accepted 3 December 1999

Key words: carbonyl carbon homonuclear isotropic mixing, flexible polypeptide chains, human prion protein, sequential NMR assignment, triple-resonance experiments

Abstract

A combination of three heteronuclear three-dimensional NMR experiments tailored for sequential resonance assignments in uniformly ^{15}N, ^{13}C-labeled flexible polypeptide chains is described. The 3D (H)N(CO-TOCSY)NH, 3D (H)CA(CO-TOCSY)NH and 3D (H)CBCA(CO-TOCSY)NH schemes make use of the favorable ^{15}N chemical shift dispersion in unfolded polypeptides, exploit the slow transverse ^{15}N relaxation rates of unfolded polypeptides in high resolution constant-time [^{1}H, ^{15}N]-correlation experiments, and use carbonyl carbon homonuclear isotropic mixing to transfer magnetization sequentially along the amino acid sequence. Practical applications are demonstrated with the 100-residue flexible tail of the recombinant human prion protein, making use of spectral resolution up to 0.6 Hz in the ^{15}N dimension, simultaneous correlation with the two adjacent amino acid residues to overcome problems associated with spectral overlap, and the potential of the presently described experiments to establish nearest-neighbor correlations across proline residues in the amino acid sequence.

Abbreviations: 2D/3D, two-/three-dimensional; FID, free induction decay; DD, dipole–dipole; CSA, chemical shift anisotropy; ct, constant time; HSQC, heteronuclear single quantum coherence; INEPT, insensitive nuclei enhanced by polarization transfer, PFG, pulse field gradient; hPrP(23–230), intact recombinant human prion protein with residues 23 to 230; TOCSY, total correlation spectroscopy.

Introduction

Sequence-specific resonance assignments are the foundation of detailed studies of biological macromolecules by NMR. Robust procedures are available for folded globular proteins, which usually show a wide dispersion of chemical shifts (Wüthrich, 1986; Bax and Grzesiek, 1993). Flexible 'unfolded' polypeptides typically have only limited ^{1}H and ^{13}C chemical shift dispersion, but they also show much slower spin relaxation rates than globular proteins. This enables the recording of more highly resolved spectra with the use of long chemical shift evolution times, and in particular with the introduction of constant-time (ct) evolution periods that produce spectra with uniform line widths determined by the length of the ct period. This paper presents NMR experiments which make use of these features and are tailored for studies of 'unfolded' flexible polypeptides that are uniformly ^{15}N, ^{13}C-labeled.

A prime motivation for this work was the special situation found with intact prion proteins in aque-

*Present address: Cellular Biochemistry and Biophysics Program, Memorial Sloan-Kettering Cancer Center, 1275 York Avenue, New York, NY 10021, U.S.A.
**To whom correspondence should be addressed. Phone: +41 1 633 2473, Fax: +41 1 633 1151.

ous solution (Donne et al., 1997; Riek et al., 1997). They are formed by two parts, a folded, globular 100-residue domain and a 100-residue flexible 'polypeptide tail'. The tail contains a 40-residue segment with five nearly identical octapeptide repeats, each of which includes four Gly and one Pro residue (Schätzl et al., 1995), and shows ^{1}H and ^{15}N chemical shifts that are very close to the corresponding random coil shifts (Bundi and Wüthrich, 1979; Braun et al., 1994). The presently introduced NMR experiments are applied to the recombinant human prion protein, hPrP(23–230), and the paper includes a report on the assignment of the NMR spectrum of the flexible tail of hPrP(23–230). Assignments of the C-terminal globular domain containing residues 121–230 were achieved for both hPrP(23–230) and hPrP(121–230) using conventional triple-resonance experiments (Bax and Grzesiek, 1993). This data has been presented jointly with the structure determination of the globular domain (Zahn et al., 2000).

Methods

When working with flexible, unfolded polypeptides one needs to exploit primarily the comparatively large dispersion of the ^{15}N chemical shifts (Braun et al., 1994; Wüthrich, 1994; Dyson and Wright, 1998) and long transverse relaxation times. To demonstrate the improved resolution available for the flexible polypeptide tail of hPrP(23–230) along the ^{15}N chemical shift dimension, we introduced a ct ^{15}N evolution period into the conventional 2D [^{1}H,^{15}N]-HSQC experiment of Bodenhausen and Ruben (1980). The improved resolution thus achieved is illustrated in Figure 1 with the resonances of the glycines, histidines and glutamines of the octapeptide repeats of hPrP(23–230). In both experiments of Figure 1 the α-carbons and the carbonyl carbons were band-selectively decoupled to avoid evolution of ^{15}N magnetization into faster relaxing antiphase states (Abragam, 1961). Depending on the decoupling schemes used, the ^{15}N transverse relaxation rates varied between 8.5 s^{-1} and 3 s^{-1} (Liu, 1999). Observations such as those in Figure 1 were the starting point for the design of the presently described high resolution NMR experiments for resonance assignments in unfolded polypeptides.

In flexible ^{13}C, ^{15}N-labelled polypeptide chains in H_2O solution studied at moderate external magnetic field strengths, the backbone carbonyl carbons have long transverse relaxation times when compared to

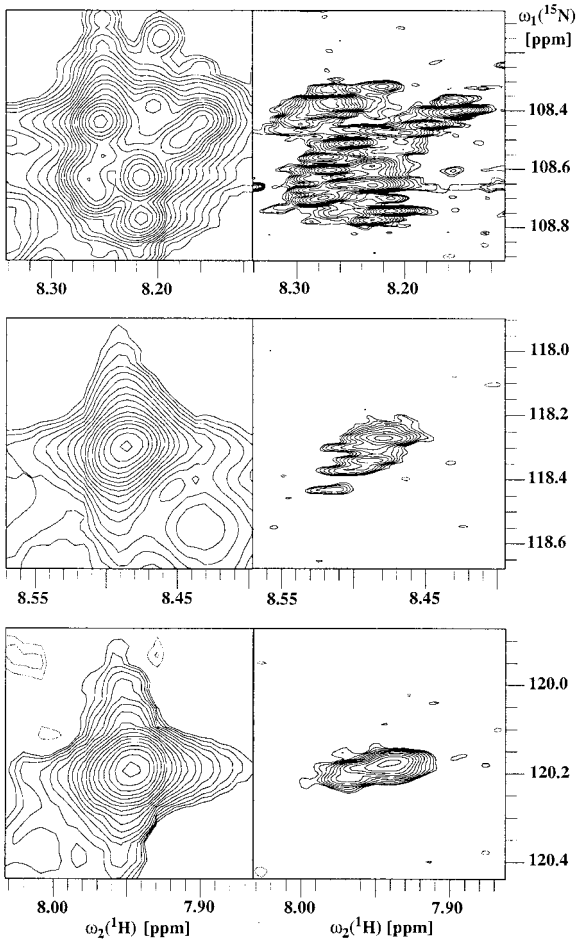

Figure 1. Comparison of a 2D [^{1}H, ^{15}N]-HSQC spectrum recorded with $t_{1,max}$ = 400 ms and 4 scans per t_1 increment (left panels), and a 2D ct-[^{1}H, ^{15}N]-HSQC spectrum (Liu, 1999) with $t_{1,max}$ = 800 ms within a constant-time period of 812 ms and 16 scans per t_1 increment (right panels). In both experiments the sample was a 1 mM solution of ^{13}C, ^{15}N-labeled hPrP(23–230) in 95% H_2O/5% D_2O at pH 4.5 and 10 °C. The spectra were recorded on a Bruker DRX 600 spectrometer, using a ^{1}H acquisition time of 286 ms. The upper, middle, and lower traces show resonances of glycines, histidines and glutamines, respectively, in the octapeptide repeats of hPrP(23–230). in both experiments a cosine window function was applied in both dimensions prior to Fourier transformation. The spectra were zero-filled from 972∗4096 complex data points to 8192∗4096 complex points (left panel) and from 1944∗4096 complex points to 8192∗4096 complex points (right panel).

the amide ^{15}N and $^{13}C^{\alpha}$ spins, since they have no directly bound protons and relax almost exclusively due to chemical shift anisotropy (CSA). Carbonyl carbon homonuclear isotropic mixing through the sequential three-bond couplings $^{3}J_{C'C'}$ is therefore a method of choice to transfer magnetization along the polypeptide backbone. $^{3}J_{C'C'}$ is related to the backbone dihe-

dral angle Φ by a Karplus-type relation (Grzesiek and Bax, 1997). To estimate the transfer efficiency for C′–C′ TOCSY one has to consider that $^3J_{C'C'}$ is averaged to about 1 Hz in flexible polypeptides such as the one studied in this paper. When employing homonuclear isotropic mixing, backbone carbonyl magnetization of a given residue is transferred with equal efficiency to both sequentially adjoining residues, which may be an advantage in crowded regions in that assignments can be tackled in two directions. The slow ^{13}CO relaxation rates further enable one to establish nearest-neighbor connectivities across proline residues, which frequently cause gaps in the sequential assignments when using conventional NMR experiments (Wüthrich, 1986; Bax and Grzesiek, 1993).

The 3D (H)N(CO-TOCSY)NH experiment

The 3D (H)N(CO-TOCSY)NH experiment correlates sequentially adjoining amide resonances through the carbonyl carbons (Figure 2a), with the ^{15}N chemical shifts dispersed in the two indirect dimensions. It differs from the COSY-type-transfer-mediated 4D HN(COCA)NH (Grzesiek et al., 1993b) and 3D (H)N(COCA)NH (Matsuo et al., 1996; Bracken et al., 1997) experiments in that sequential connectivities are established in both directions, which may provide more reliable assignments in the case of partial resonance degeneracy. Using carbonyl carbon isotropic mixing, as previously employed in the 3D (HN)CO(CO)NH experiment (Grzesiek and Bax, 1997), the new experiment transfers magnetization between adjacent backbone carbonyl carbons twice as fast as COSY-type transfers (Braunschweiler and Ernst, 1983). Aliphatic carbon ($^{13}C^{ali}$) band-selective decoupling keeps the magnetization components in-phase with respect to aliphatic carbons and thus avoids evolution to more rapidly relaxing antiphase states (band-selective $^{13}C^{ali}$ decoupling cannot be applied in the aforementioned 3D (H)N(COCA)NH experiment, which may cause significant additional sensitivity losses during the 50 ms ^{15}N evolution period). The 3D (H)N(CO-TOCSY)NH experiment further correlates the side chain amide ^{15}N of Asn with the backbone amide group of the sequentially succeeding residue through the intraresidual three-bond coupling between the Asn side chain carbonyl carbon and the backbone carbonyl carbon, $^3J_{COC'}$. This provides a unique 'fingerprint' of Asn residues, which supports the establishment of sequence-specific assignments, and further identifies the correlation direction towards

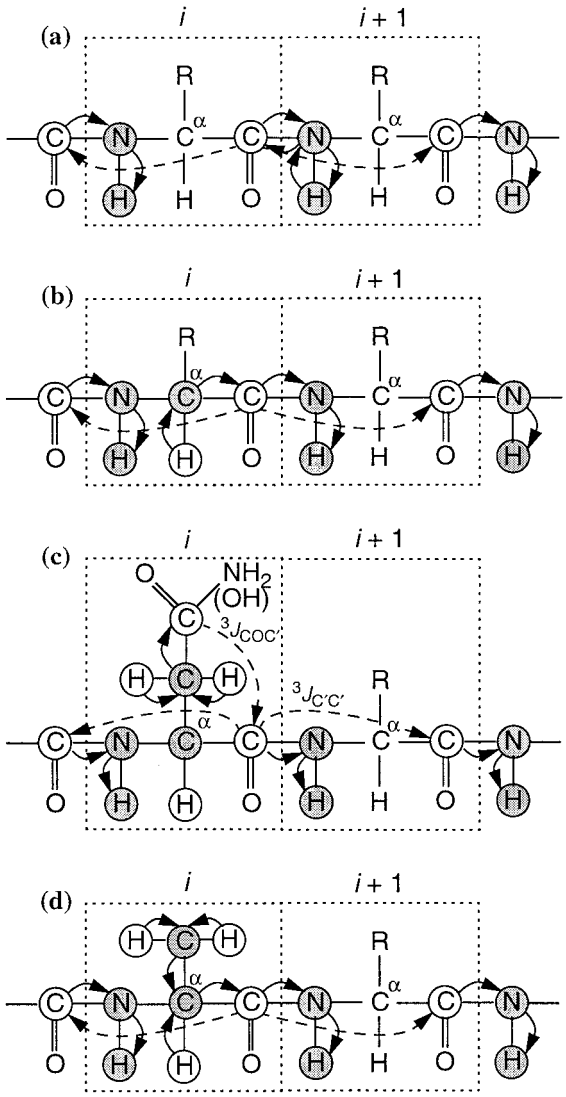

Figure 2. Dipeptide backbone fragment of residues *i* and $i + 1$. R represents amino acid side chains. Magnetization transfers by INEPT or by COSY-type processes are indicated by solid arrows, and magnetization transfers through carbonyl homonuclear isotropic mixing by dashed arrows. Spins involved only in magnetization transfer are encircled, and those that are also frequency-labeled are drawn with a grey background. (a) Magnetization transfer pathway in the 3D (H)N(CO-TOCSY)NH experiment and its 2D version, with the amide proton of residue $i + 1$ as the starting point. (b) Magnetization transfer in the 3D (H)CA(CO-TOCSY)NH experiment, with the $^1H^\alpha$ magnetization of residue *i* as the starting point. (c) Same as (b), showing the magnetization transfer pathway that starts with $^1H^\beta$ of Asn or Asp in position *i* and is propagated through side chain CO-to-backbone carbonyl homonuelear isotropic mixing. (d) Magnetization transfer in the 3D (H)CBCA(CO-TOCSY)NH experiment, with the $^1H^\alpha$ and $^1H^\beta$ magnetizations of residue *i* as the starting points.

the C-terminus in this otherwise symmetric correlation strategy.

The magnetization transfer pathway of the 3D (H)N(CO-TOCSY)NH experiment (Figure 2a) is

$$^{1}H^{N} \rightarrow ^{15}N(t_1) \rightarrow ^{13}C'\text{-(isotropic mixing)} \rightarrow ^{13}C' \rightarrow ^{15}N(t_2) \rightarrow ^{1}H^{N}(t_3), \quad (1)$$

where $^{1}H^{N}$, ^{15}N, and $^{13}C'$ stand for amide protons, amide nitrogens and carbonyl carbons, t_1 and t_2 indicate the ^{15}N evolution periods, and t_3 is the detection period of the proton magnetization. The experiment starts with polarization of the amide proton of residue $i + 1$, which is transferred to the directly attached amide nitrogen by an INEPT step (Morris and Freeman, 1979) at time point *a* (Figure 3). A ct evolution period t_1 (Santoro and King, 1992; Vuister and Bax, 1992) follows between the time points *a* and *b*. At point *b* the $^{15}N(i + 1)$ magnetization is in-phase with respect to $^{1}H^{N}(i + 1)$ and antiphase with respect to $^{13}C'(i)$. It is transferred to $^{13}C'(i)$ through a pair of 90° pulses on ^{15}N and $^{13}C'$ at points *b* and *c*, and refocused with respect to $^{15}N(i + 1)$ at point *d*. Subsequently, the in-phase $^{13}C'(i)$ magnetization is used for homonuclear isotropic mixing with a DIPSI-3 sequence (Shaka et al., 1988; Wider, 1998), which promotes transfer to the sequentially adjacent carbonyl carbons, $^{13}C'(i - 1)$ and $^{13}C'(i + 1)$. Between the time points *e* and *f* the $^{13}C'$ magnetizations are transformed to antiphase with respect to the directly attached ^{15}N spins, and then transferred to ^{15}N by the two 90° pulses at points *f* and *g*. This is followed by the second ^{15}N ct evolution period from time points *g* to *h*. During this period the ^{15}N magnetization becomes in-phase with respect to $^{13}C'$ and antiphase with respect to its $^{1}H^{N}$. Finally, the ^{15}N magnetization is transferred back to $^{1}H^{N}$ by a PFG coherence selection scheme (Muhandiram and Kay, 1993), and the proton magnetization is detected during the acquisition period t_3.

If residue $i + 1$ is Asn, the side chain $^{1}H^{N}(i + 1)$ and $^{15}N(i + 1)$ magnetizations are transferred intraresidually to the side chain $^{13}CO(i + 1)$. During the carbonyl homonuclear isotropic mixing the side chain $^{13}CO(i + 1)$ magnetization is then further transferred intraresidually to the backbone carbonyl carbon, $^{13}C'(i + 1)$. A pair of pulsed field gradients flank the isotropic mixing period to purge unwanted magnetization during the z-filter (Sørensen et al., 1984; Rance, 1987; Wider, 1998). Delays or initial values of the evolution periods τ, δ, η, *D* and *E* are set for maximal signal sensitivity, which is a compromise between maximum defocusing/refocusing of the ^{15}N and $^{13}C'$ magnetizations and minimal losses due to transverse relaxation (see caption to Figure 3). Aliphatic carbons are band-selectively decoupled during most of the pulse sequence to avoid unwanted antiphase states with $^{13}C^{ali}$ spins, which results in enhanced sensitivity when compared to an individual 180° inversion pulse for $^{13}C^{ali}$ decoupling.

For the assignments in hPrP(23–230) a 2D version of the experiment of Figure 3 has also been used, with $t_2 \equiv 0$, to achieve very high resolution along ω_1 (^{15}N) (Liu, 1999).

The 3D (H)CA(CO-TOCSY)NH and 3D (H)CBCA(CO-TOCSY)NH experiments

The 3D (H)CA(CO-TOCSY)NH experiment (Figure 4a) derives from the 3D (H)N(CO-TOCSY)NH scheme by replacement of t_1 (^{15}N) by a carbon evolution period. The resulting experiment then correlates on the one hand the $^{13}C^{\alpha}(i)$ chemical shifts with the amide moieties of the residues *i*, $i + 1$ and $i + 2$ (Figure 2b). On the other hand the $^{13}C^{\beta}$ shifts of Asn and Asp residues in position *i* are correlated with the amide moieties of the residues *i*, $i + 1$ and $i + 2$ by the carbonyl carbon TOCSY transfer from the side chain ^{13}CO to the backbone $^{13}C'$ spins of the residues *i*, $i - 1$ and $i + 1$, making use of the three-bond couplings $^{3}J_{COC'}$ and $^{3}J_{C'C'}$ (Figure 2c). Thus the (H)CA(CO-TOCSY)NH spectrum also shows 'fingerprint' sequential connectivities with Asn and Asp β-carbons. In the 3D (H)CBCA(CO-TOCSY)NH experiment (Figure 4b) an additional COSY-step ensures that the C^{β}-carbons are included into the correlation for all residues, which provides connectivities of the amide moieties *i*, $i + 1$ and $i + 2$ with $^{13}C^{\beta}(i)$, in addition to the connectivities with $^{13}C^{\alpha}(i)$ (Figure 2d). The experiments of Figure 4 afford sequential connectivities in both directions, and compared to the information obtained with HN(CO)CA (Bax and Ikura, 1991) and CBCA(CO)NH (Grzesiek and Bax, 1992) this may in some instances help to overcome signal degeneracy in unfolded polypeptides. They also provide unique connectivities between the residues *i* and $i + 2$ in case residue $i + 1$ is a proline, which otherwise usually breaks the sequential connectivities obtainable with conventional $^{1}H^{N}$-detected triple-resonance experiments.

The magnetization transfer pathways of the 3D (H)CA(CO-TOCSY)NH and 3D (H)CBCA(CO-TOCSY)NH experiments (Figure 2, b–d) can be de-

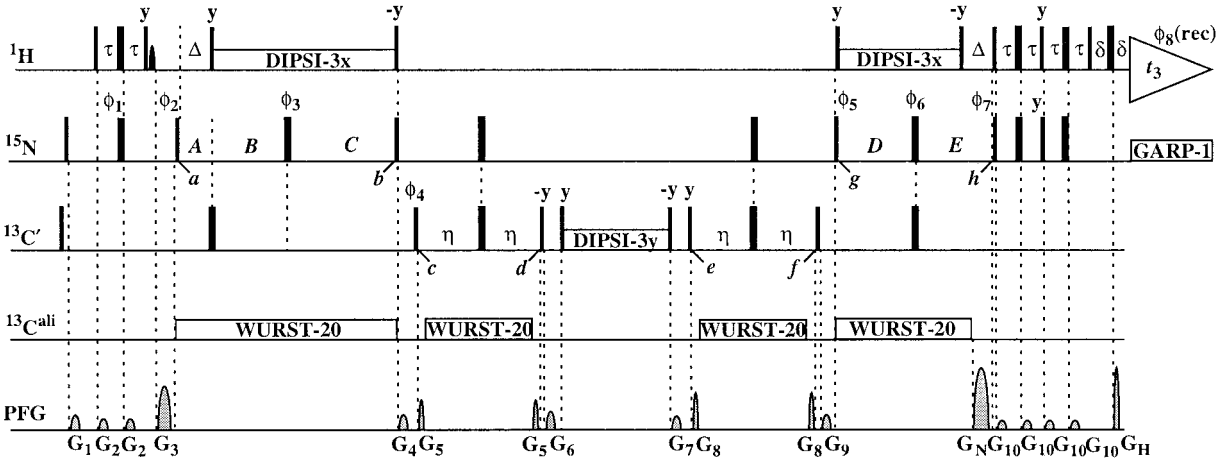

Figure 3. Pulse sequence for the 3D (H)N(CO-TOCSY)NH experiment. Narrow and wide rectangular black bars indicate non-selective 90° and 180° pulses, respectively. Unless indicated otherwise, the pulses are applied with phase x. The ^{1}H and ^{15}N carrier frequencies are set at 4.78 ppm (water) and 117.5 ppm, respectively. The ^{13}C carrier frequency is set at 175.5 ppm for carbonyl carbons and at 42.0 ppm for aliphatic carbons. The non-selective proton pulses are applied using a 30.1 kHz field strength. The selective ^{1}H 90° pulse used for water flip-back (Grzesiek and Bax, 1993) during the first INEPT transfer (Morris and Freeman, 1979) is applied for a duration of 2 ms with the SEDUCE-1 profile (McCoy and Mueller, 1992, 1993). The ^{15}N pulses are applied with a field strength of 6.25 kHz. Proton decoupling using the DIPSI-3x sequence (Shaka et al., 1988; Wider, 1998) with a field strength of 3.57 kHz is applied during most of the t_1 and t_2 evolution periods, and ^{15}N decoupling using the GARP-1 sequence (Shaka et al., 1985; Wider, 1998) with 1.0 kHz is applied during acquisition. The strength of the ^{13}C′ pulses is adjusted so that they cause minimal excitation of aliphatic carbons (^{13}C^{ali}) (Kay et al., 1990). ^{13}C^{ali} band-selective decoupling is achieved with the adiabatic decoupling sequence WURST-20 (Kupče and Freeman, 1995), using a 2 ms pulse length, 20 kHz sweep-width, 1.96 kHz amplitude, and applying a 5-STEP super phase cycle (Tycko et al., 1985) to reduce decoupling side-bands. The decoupling of ^{13}C^{ali} is switched off during the application of pulsed field gradients. ^{13}C′ homonuclear isotropic mixing is achieved using DIPSI-3y (Shaka et al., 1988; Wider, 1998), with a field strength of 2.2 kHz (90° pulse of 113.2 μs) and a mixing time of 124 ms. The delays are $\tau = 2.73$ ms, $\Delta = 5.5$ ms, $\delta = 0.4$ ms, and $\eta = 14.0$ ms. The initial values of the individual periods containing t_1 and t_2 are: $A(t_1 = 0) = 14.0$ ms, $C(t_1 = 0) = 54.0$ ms, $D(t_2 = 0) = 14.0$ ms, $E(t_2 = 0) = 14.0$ ms; $B = 40.0$ ms. The t_1 chemical shift evolution periods, *A* and *C*, are incremented and decremented, respectively, by $C(t_1 = 0)/\kappa_1$, with $\kappa_1 = \mathrm{SW}_1 \times (A + B + C)$. The t_2 chemical shift evolution periods, *D* and *E*, are incremented and decremented by $D(t_2 = 0)/\kappa_2$, with $\kappa_2 = \mathrm{SW}_2 \times (D + E)$. SW_1 and SW_2 are the spectral widths in the ω_1 and ω_2 dimensions. The phase cycling scheme employed is ϕ_1 = x; ϕ_2 = x, −x; ϕ_3 = 2(x), 2(y), 2(−x), 2(−y); ϕ_4 = 2(x), 2(−x); ϕ_5 = 4(x), 4(−x); ϕ_6 = 2(x), 2(−x); ϕ_7 = x; ϕ_8(rec) = x, −x, x, −x, −x, −x, x. Quadrature detection in the ω_1 (^{15}N) dimension is achieved with States-TPPI (Marion et al., 1989), where the phase ϕ_2 is increased together with ϕ_1. For each value of t_2, N- and P-type coherences are obtained by recording two data sets, whereby the sign of the gradient G_H and the phase ϕ_7 are inverted for the second data set. Data sets obtained in an interleaved manner for positive and negative G_H values are stored in separate memory locations, and pure absorptive line shapes in the ω_2(^{15}N) dimension are generated by constructive shuffling of the N- and P-type data sets (Cavanagh et al., 1991; Kay et al., 1992). Residual water magnetization is suppressed by PFG coherence selection. The durations and strengths of the sine-shaped z-axis pulsed field gradients are: G_1, 0.8 ms, 10 G/cm; G_2, 0.5 ms, 7 G/cm; G_3, 1.45 ms, 30 G/cm; G_4, 0.7 ms, 10 G/cm; G_5, 0.2 ms, 20 G/cm; G_6, 0.8 ms, 12 G/cm; G_7, 0.8 ms, 9 G/cm; G_8, 0.2 ms, 25 G/cm; G_9, 0.6 ms, 10 G/cm; G_{10}, 0.75 ms, 6 G/cm; G_N, 1.75 ms, 42 G/cm; G_H, 0.1773 ms, 42 G/cm. In the 2D (H)N(CO-TOCSY-N)H experiment, *D* and *E* are kept constant, so that there is magnetization transfer from ^{15}N to ^{1}H^N but no second ^{15}N chemical shift labeling.

scribed by Equations 2 and 3.

$$^1\mathrm{H}^{\alpha} \rightarrow {}^{13}\mathrm{C}^{\alpha}(t_1) \rightarrow {}^{13}\mathrm{C}'\text{-(isotropic mixing)} \rightarrow {}^{13}\mathrm{C}' \rightarrow {}^{15}\mathrm{N}(t_2) \rightarrow {}^1\mathrm{H}^{\mathrm{N}}(t_3), \quad (2)$$

$$^1\mathrm{H}^{\alpha/\beta} \rightarrow {}^{13}\mathrm{C}^{\alpha/\beta} \rightarrow {}^{13}\mathrm{C}^{\alpha}(t_1) \rightarrow {}^{13}\mathrm{C}'\text{-(isotropic mixing)} \rightarrow {}^{13}\mathrm{C}' \rightarrow {}^{15}\mathrm{N}(t_2) \rightarrow {}^1\mathrm{H}^{\mathrm{N}}(t_3) \quad (3)$$

The same notation is used as in Equation 1 with ^{1}H$^{\alpha}$, ^{1}H$^{\alpha/\beta}$, ^{13}C$^{\alpha}$, ^{13}C$^{\beta}$ and ^{13}C$^{\alpha/\beta}$ denoting α-protons, α- and β-protons, α-carbons, β-carbons, and α- and β-carbons, respectively. The magnetization transfer processes derive from the CBCA(CO)NH experiment (Grzesiek and Bax, 1992), and from the (H)N(CO-TOCSY)NH experiment presented in the previous section. In (H)CA(CO-TOCSY)NH (Figure 4a), magnetization is transferred at time point *a* from aliphatic protons of residue *i* to their attached ^{13}C spins. Between time points *a* and *b*, transverse ^{13}C(*i*) magnetization is subject to a ct evolution period (Santoro and King, 1992; Vuister and Bax, 1992) and evolves into antiphase either with respect to the attached backbone carbonyl carbon for ^{13}C$^{\alpha}$(*i*) (Figure 2b) or with respect to the side chain ^{13}CO(*i*) for ^{13}C$^{\beta}$(*i*) of Asn

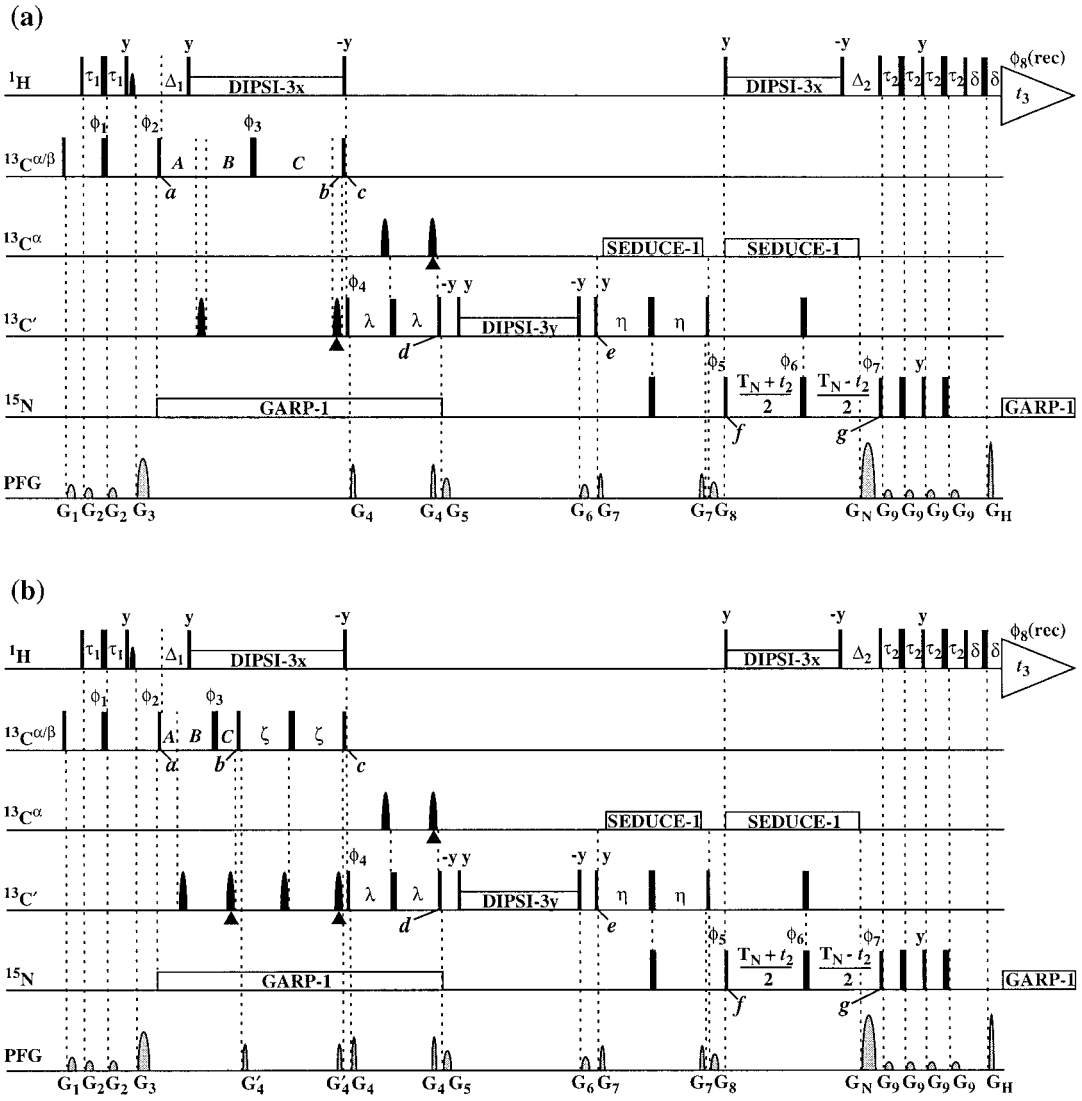

Figure 4. Pulse sequences for the 3D (H)CA(CO-TOCSY)NH and 3D (H)CBCA(CO-TOCSY)NH experiments. Unless indicated otherwise, notations, field strengths, and offsets of pulses and decoupling sequences are the same as in Figure 3. In (a) the ^{13}C carrier frequency is set to 42.0 ppm at the start of the pulse sequence and then switched to 56 ppm at time point *c*. $^{13}C^{\alpha}$ band-selective decoupling is achieved using the WALTZ-16 sequence (Shaka et al., 1983; Wider, 1998) with SEDUCE-1 (255.7 μs pulse length) (McCoy and Mueller, 1992), which is switched off during the application of pulsed field gradients. The strengths of the $^{13}C^{\alpha/\beta}$ hard pulses are adjusted to minimize excitation of $^{13}C'$, and vice versa (Kay et al., 1990). The selective 180° pulses indicated by shaped bars on the ^{13}C channels are applied with a Gaussian profile truncated at 5% and a pulse length of 100 μs. Pulses that are applied to compensate for non-resonant effects are indicated with a ▲ sign. The delays are $\tau_1 = 1.8$ ms, $\tau_2 = 2.73$ ms, $\Delta_1 = 2.2$ ms, $\Delta_2 = 5.5$ ms, $\delta = 0.4$ ms, $\lambda = 4.5$ ms, $\eta = 14.0$ ms, and $T_N = 28.0$ ms. The initial values of the individual periods containing t_1 are either $A(t_1 = 0) = 4.0$ ms, $C(t_1 = 0) = 4.0$ ms, with $B = 0$ for a 'low resolution' spectrum (see text), or $A(t_1 = 0) = 4.5$ ms, $C(t_1 = 0) = 13.5$ ms, with $B = 9.0$ ms for a 'high resolution' spectrum. *A* and *C* are incremented and decremented, respectively, by $C(t_1 = 0)/\kappa$, with $\kappa = SW_1 \times (A + B + C)$, where SW_1 is the ^{13}C spectral width. The phase cycling is ϕ_1 = x; ϕ_2 = x, −x; ϕ_3 = 2(x), 2(−x), 2(y), 2(−y); ϕ_4 = 2(x), 2(−x); ϕ_5 = x; ϕ_6 = 4(x), 4(−x); ϕ_7 = x; ϕ_8(rec) = x, −x, −x, x, −x, x, x, −x. Quadrature detection in the ω_1 (^{13}C) dimension is achieved with States-TPPI (Marion et al., 1989), where the phase ϕ_2 is shifted together with ϕ_1. For each value of t_2, N- and P-type coherences are obtained by recording two data sets, whereby the sign of the gradient G_H and the phase ϕ_7 are inverted for the second data set. Data sets obtained in an interleaved manner for positive and negative G_H values are stored in separate memory locations, and pure absorptive line shapes in the ω_2(^{15}N) dimension are generated by constructive shuffling of the N- and P-type data sets (Cavanagh et al., 1991; Kay et al., 1992). Residual water magnetization is suppressed by PFG coherence selection. The durations and strengths of the sine-shaped z-axis pulsed field gradients are G_1, 0.8 ms, 10 G/cm; G_2, 0.5 ms, 7 G/cm; G_3, 1.45 ms, 30 G/cm; G_4, 0.2 ms, 25 G/cm; G_5, 0.7 ms, 15 G/cm; G_6, 0.7 ms, 10 G/cm; G_7, 0.2 ms, 18 G/cm; G_8, 0.6 ms, 12 G/cm; G_9, 0.75 ms, 6 G/cm; G_N, 1.75 ms, 42 G/cm; G_H, 0.1773 ms, 42 G/cm. In (b), the delay $\zeta = 4.2$ ms. The initial values of the individual periods containing t_1 are $A(t_1 = 0) = 0$, $C(t_1 = 0) = 3.5$ ms, with $B = 3.5$ ms. There are two additional gradients G'_4, 0.2 ms, 20 G/cm. All the other parameters are the same as in (a).

or Asp (Figure 2c). At time point *c*, aliphatic ^{13}C magnetization is transferred from $^{13}C^{\alpha}$ to $^{13}C'(i)$ and from $^{13}C^{\beta}$ of Asn and Asp to the side chain $^{13}CO(i)$, and refocused with respect to the directly attached aliphatic carbon between points, *c* and *d*. During the following isotropic carbonyl mixing period the magnetization of $^{13}C'(i)$ is transferred to the carbonyls of the sequentially adjacent residues $i-1$ and $i+1$ through the three-bond couplings $^{13}J_{C'C'}$ (Figure 2b), and the side chain $^{13}CO(i)$ magnetization of the Asn and Asp residues is transferred to $^{13}C'(i)$ and then relayed to the carbonyl carbons of the adjacent residues $i-1$ and $i+1$ (Figure 2c). Subsequently, at point *f*, the $^{13}C'$ magnetization is transferred to the directly bound amide ^{15}N, where it is subjected to the ct evolution period t_2 (^{15}N) between points *f* and *g*. As in Figure 3, ^{15}N magnetization is then transferred back to $^{1}H^{N}$ for detection. $^{13}C^{ali}$ band-selective homonuclear decoupling is used during most of the period from points *e* to *g* to reduce relaxation and enhance sensitivity (Figure 4a). In two variant set-ups, a 'high resolution' spectrum is obtained by setting the constant-time evolution period for ^{13}C, A+B+C in Figure 4a, to 27.0 ms for complete refocusing of aliphatic carbon homonuclear one-bond couplings, and for a 'low resolution' spectrum this period is set to 8.0 ms, which is a compromise between optimal magnetization transfer and optimal resolution.

In the (H)CBCA(CO-TOCSY)NH experiment (Figures 2d and 4b) the magnetization transfer pathway is exactly as in (H)CA(CO-TOCSY)NH, except that an additional COSY-type step between time points *b* and *c* is inserted to transfer magnetization from $^{13}C^{\beta}$ to $^{13}C^{\alpha}$. Only a 'low resolution' version of this experiment has been implemented, with the ^{13}C evolution period, A+B+C in Figure 4b, set to 7.0 ms, which is a compromise between optimal magnetization transfer from $^{13}C^{\beta}$ and optimal use of the magnetization on $^{13}C^{\alpha}$.

Sample preparation and NMR spectrometer set-ups

The cloning, expression, and purification of ^{13}C, ^{15}N-labelled recombinant hPrP(23–230) has been carried out as described (Zahn et al., 1997), except that some modifications were introduced in the purification procedure. A freshly transformed overnight culture of *Escherichia coli* BL21(DE3) cells (Stratagene) containing the plasmid for expression of hPrP(23–230) at 37 °C was added to 4 litres of minimal medium containing 1 g/l of [^{15}N]-ammonium chloride, 2 g/l of [$^{13}C_6$]-glucose, a vitamin cocktail (5 mg/l thiamine, 1 mg/l d-biotin, 1 mg/l choline chloride, 1 mg/l folic acid, 1 mg/l niacinamide, 1 mg/1 D-phantothenic acid, 1 mg/l pyridoxal hydrochloride, 0.1 mg/l riboflavin) and 100 μg/ml ampicillin. At $OD_{600} = 1$, expression of hPrP(23–230) into inclusion bodies was induced with isopropyl β-D-thiogalactopyranoside to 1 mM final concentration. The cells were harvested after growing for 8 h at 37 °C, centrifuged, and resuspended in 100 ml buffer G (6 M GdmCl, 10 mM TrisHCl, 100 mM Na_2PO_4, 10 mM reduced glutathione, pH 8.0). After sonication and centrifugation, the soluble protein fraction was added to 20 ml of nickel-nitrilotriacetic acid agarose resin (Quiagen) and stirred for 1 h at room temperature. The resin was poured into a column and washed with 120 ml buffer G. In order to prevent unspecific binding of proteins devoid of histidine tails, 10 mM imidazole was added to the buffer G. To the immobilized histidine tail-containing fusion protein we applied a 200 ml gradient of buffer G to buffer B (10 mM TrisHCl, 100 mM Na_2PO_4, 10 mM imidazole, pH 8.0). After washing with 40 ml of buffer B, the hPrP(23–230) polypeptides were eluted with 150 ml buffer B containing 500 mM imidazole and titrated to pH 5.8. The resin was rinsed with 40 ml of buffer B, and oxidative refolding and imidazole elution were repeated three times to obtain additional batches of soluble prion protein. After dialysing the histidine tail-fused hPrP(23–230) against water, the histidine tail was removed from the prion protein using thrombin (Sigma, 1 unit/μmol of protein). The cleaving reaction was carried out at room temperature overnight in 5 mM TrisHCl buffer at pH 8.2. The protease was removed from hPrP(23–230) by loading onto a CM 52 column (25 g resin; Whatman) equilibrated in the same buffer, followed by elution with a 200 ml gradient from 0 to 500 mM NaCl. The cleaved histidine tail was removed by dialysis against water using a Spectrapor membrane (MW 3500–8000). The cleavage site of the histidine tail introduces an additional Gly-Ser dipeptide segment at the N-terminus of the purified protein, which was documented by SDS-polyacrylamide gel electrophoresis, N-terminal sequencing, and MALDI. Concentrated protein solutions for NMR spectroscopy were obtained using an Ultrafree-15 Centrifugal Filter Device (Millipore).

Unless mentioned otherwise, all spectra were acquired at 20 °C with a 1 mM solution of ^{13}C, ^{15}N-labelled hPrP(23–230) in 93% H_2O/7% D_2O containing 10 mM sodium acetate and 0.05% sodium azide at pH 4.5. All experiments were performed on a Bruker DRX600 spectrometer equipped with triple resonance

z-gradient probes. The time-domain data sets were processed using the program PROSA (Güntert et al., 1992) and the spectra were analysed using the program XEASY (Bartels et al., 1995).

Results and discussion

Obtaining resonance assignments of the flexible tail in hPrP(23–230) is the basis for detailed dynamic or conformational studies (Wüthrich, 1986). This task is not straightforward in view of the previously mentioned facts that the resonances in the tail exhibit mostly random-coil chemical shifts, and that the tail contains a sequence of five octapeptide repeats, each of which contains four Gly and one Pro. In the following, the novel high resolution correlation experiments introduced in the Methods section are applied with hPrP(23–230) in an attempt to obtain the desired assignments.

Backbone amide resonance assignments of the tail of hPrP(23–230)

$\omega_3(^1H)/\omega_1(^{15}N)$ strips from a 3D (H)N(CO-TOCSY)-NH spectrum of hPrP(23–230) taken through the ^{15}N diagonal peaks in the $\omega_1(^{15}N)/\omega_2(^{15}N)$ plane show the sequential amide–amide connectivities from residues Trp 89 to Lys 101 (Figure 5). Some weak relay peaks also indicate longer-range connectivities, which is a valuable additional feature for obtaining unambiguous assignments. Quite generally, the bidirectional sequential correlation achieved with the 3D (H)N(CO-TOCSY)NH experiment is useful to resolve resonance overlap. For example, in Figure 5 the amide resonances of Gly 93 and Gly 94 are almost completely overlapped. Nonetheless, since in the 3D (H)N(CO-TOCSY)NH spectrum the amide resonances of Gly 93 and Gly 94 are also correlated with the resolved amide resonances of, respectively, Gly 92 in its strip and Thr 95 in its strip, the assignment is facilitated. The peak labeled with an asterisk in the strip for Lys 101 (Figure 5) shows a side chain correlation peak, where the side chain amide ^{15}N of Asn 100 is correlated with the backbone amide resonance of Lys 101. This Asn 'fingerprint' identifies the direction toward the C-terminus for this otherwise bidirectional correlation technique. In the tail of hPrP(23–230) the side chain correlation peaks have been observed for all four Asn residues, thus yielding also assignments for the Asn side chain amide resonances.

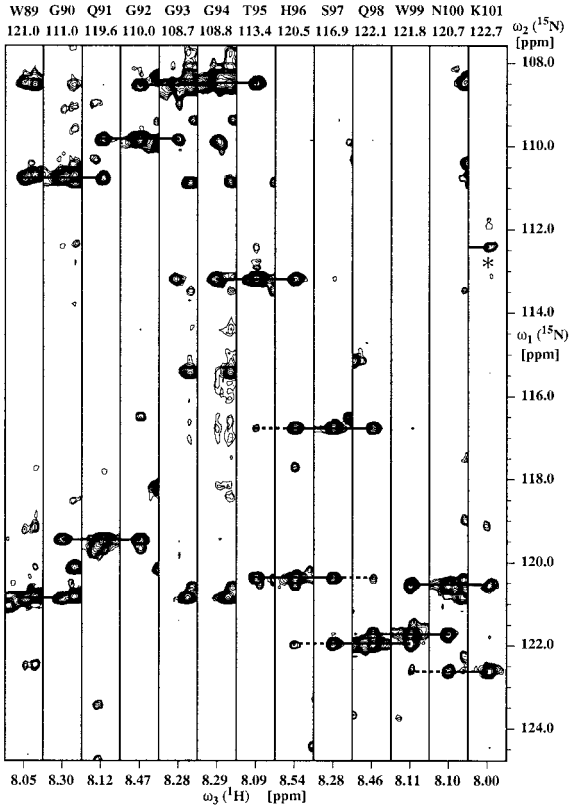

Figure 5. $\omega_3(^1H)/\omega_1(^{15}N)$ strips from a 3D (H)N(CO-TOCSY)NH spectrum of hPrP(23–230) taken through the ^{15}N diagonal peaks in the $\omega_1(^{15}N)/\omega_2(^{15}N)$ plane. Along $\omega_3(^1H)$ the strips are 0.117 ppm wide and are centered about the amide proton shift. The experiment was performed on a Bruker DRX 600 spectrometer using a 1 mM solution of ^{13}C, ^{15}N-labeled hPrP(23–230) in 93% H_2O/7% D_2O at pH 4.5 and 20 °C. Eight scans were accumulated per t_1 increment, resulting in 58 h of measuring time. Sequential connectivities are shown by solid lines and longer-range connectivities by dashed lines. The sequential peak from the side chain amide group of Asn 100 in the strip of Lys 101 is indicated by an asterisk (see text and Figure 2).

For part of the hPrP(23–230) tail a high resolution 2D version of the experiment of Figure 3, with $t_2(^{15}N) \equiv 0$, was helpful to resolve near-degeneracy of the chemical shifts. Figure 6 shows regions of 2D (H)N(CO-TOCSY-N)H and 2D ct-[^1H, ^{15}N]-HSQC spectra of hPrP(23–230) recorded with a maximal time of 800 ms in the ^{15}N ct evolution period. The spectra contain the amide resonances of the residues Gln 52 to Gln 59, which constitute the first of the aforementioned five octapeptide repeats. These data illustrate again that the bidirectional correlations, here in the 2D (H)N(CO-TOCSY-N)H spectrum, make it easier to connect resonances in crowded regions. For example, starting with Gln 52, which follows a pro-

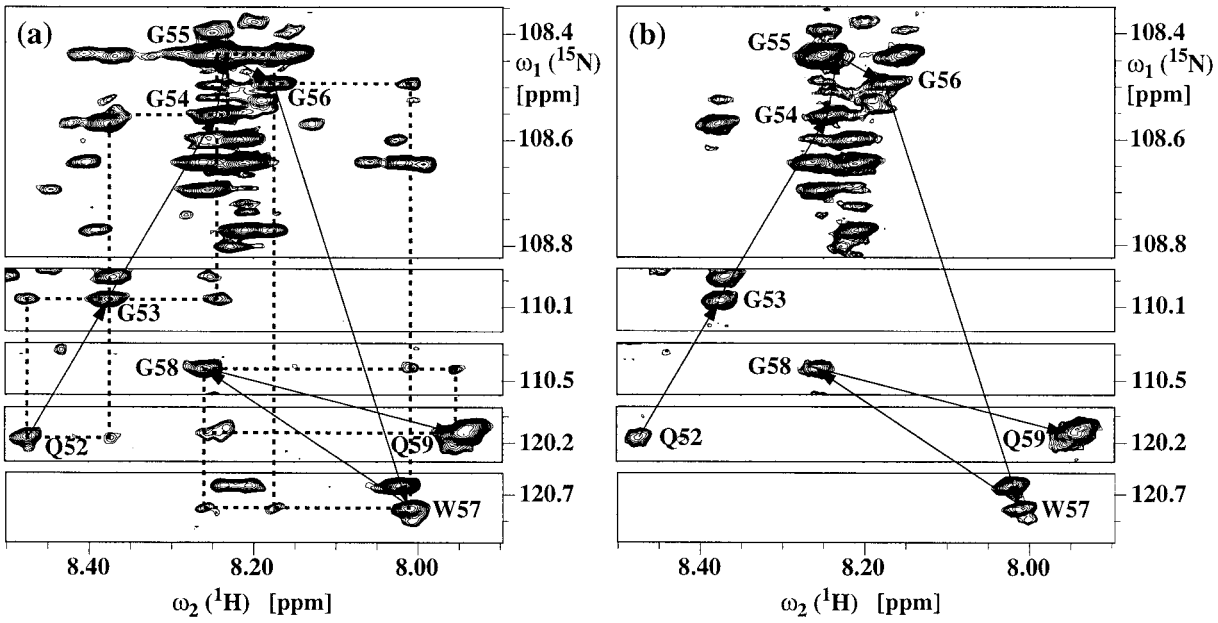

Figure 6. (a) 2D (H)N(CO-TOCSY-N)H spectrum recorded using the pulse sequence of Figure 3. (b) 2D *ct*-[^{1}H, ^{15}N]-HSQC spectrum recorded as described by Liu (1999). Both spectra were collected with a ^{15}N evolution time of 800 ms on a Bruker DRX 600 spectrometer using the same sample as in Figure 5. For (a), 68 scans per t_1 increment were recorded, resulting in 68 h of measuring time, for (b) 16 scans per t_1 increment, with a measuring time of 17 h. In (a), sequential connectivities for the residues Gln 52 to Gln 59, which constitute the first of the five octapeptide repeats in hPrP(23–230), are highlighted by dashed lines, and auto-peaks are linked by solid lines. In (b), the peaks have been similarly connected, based on the data of (a).

line in the sequence, a correlation to Gly 53 is found with a single pair of cross peaks. Gly 54 and Gly 56 can be unambiguously assigned by connecting their resonances to those of Gly 53 and Trp 57, respectively, although one of the Gly 53/Gly 54 correlation peaks is partially overlapped with the auto-peak of Gly 114. Then, Gly 55 can be identified by correlating its auto-peak with Gly 56, although its chemical shifts are nearly identical with those of other Gly residues. Finally, Gln 59 could be assigned through its connection with Gly 58, even though it is almost completely overlapped with three other Gln resonances from octapeptide repeats.

$^{13}C^{\alpha}$ and $^{13}C^{\beta}$ resonance assignments of the tail of hPrP(23–230)

Figures 7a and b show $\omega_3(^1\mathrm{H})/\omega_1(^{13}\mathrm{C}^{\alpha/\beta})$ strips from a 3D (H)CA(CO-TOCSY)NH spectrum recorded with a $t_1(^{13}\mathrm{C})$ evolution time of 27.0 ms, and a 3D (H)CBCA(CO-TOCSY)NH spectrum with a $t_1(^{13}\mathrm{C})$ evolution time of 7.0 ms, respectively, which establish sequential $^{13}\mathrm{C}^{\alpha/\beta}$-to-amide connectivities in the polypeptide segment from residues Asn 100 to Lys 110. The strong direct correlation peaks give the same information as in 3D HN(CO)CA (Bax and Ikura, 1991) and 3D CBCA(CO)NH (Grzesiek and Bax, 1992). However, with the new experiments of Figure 4 the connectivities can be established on a more reliable basis, since in addition to the sequential correlation peaks there are also 'bridge peaks', which correlate directly the residues i and $i + 2$. The bridge peaks can provide assignments even when the sequential peaks are degenerate, and they also yield assignments for residues that are followed by proline. For example, in the strips of the 3D (H)CA(CO-TOCSY)NH spectrum the bridge peaks from Lys 101 and Lys 104 to Ser 103 and Lys 106, respectively, give unambiguous assignments (Figure 7a). In the 3D (H)CBCA(CO-TOCSY)NH spectrum the bridge peaks are weaker (Figure 7b), owing to the lower sensitivity of this experiment, which on the other hand shows additional sequential connectivities from the β-carbons. Interestingly, for residue Asn 108 the 3D (H)CA(CO-TOCSY)NH spectrum of Figure 7a shows both sequential and bridge peaks from $^{13}\mathrm{C}^{\beta}$, which is the result of magnetization starting at the $^1\mathrm{H}^{\beta}$ protons and being transferred through $^{13}\mathrm{C}^{\beta}$ to the side chain carbonyl carbon before the start of the homonuclear isotropic mixing (see Figure 2c).

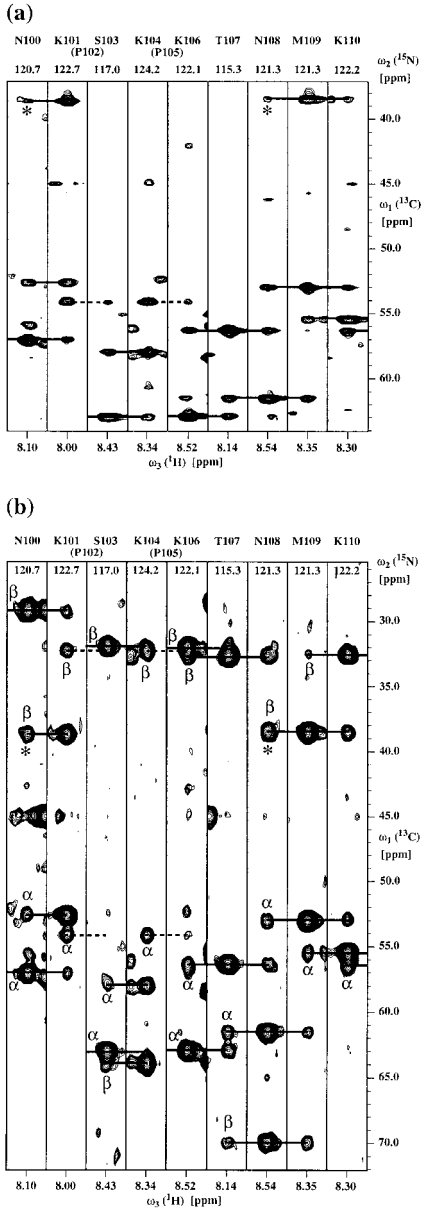

Figure 7. (a) $\omega_3(^1H)/\omega_1(^{13}C^{\alpha})$ strips from a high resolution 3D (H)CA(CO-TOCSY)NH spectrum of hPrP(23–230) recorded with a $t_1(^{13}C)$ evolution time of 27.0 ms. (b) $\omega_3(^1H)/\omega_1(^{13}C^{\alpha/\beta})$ strips from a 3D (H)CBCA(CO-TOCSY)NH spectrum of hPrP(23–230) recorded with a $t_1(^{13}C)$ evolution time of 7.0 ms. Along $\omega_3(^1H)$ the strips are 0.117 ppm wide and are centered about the amide proton shift. Both spectra were collected on a Bruker DRX 600 spectrometer with the same sample as in Figure 5. For (a), 4 scans per t_1 increment were recorded, resulting in 49 h of measuring time, for (b) 4 scans per t_1 increment gave a measuring time of 13 h. Sequential peaks and longer-range 'bridge peaks' (see text) are connected with solid lines. Where the sequential connectivities are interrupted by prolines, the i to $i + 2$ connectivities are drawn with dashed lines. Sequential connectivities with Asn side chain amide groups are indicated with asterisks. In (b), α and β stand for α- and β-carbon resonances, respectively.

Proline backbone amide ^{15}N resonance assignments in the tail of hPrP(23–230)

Backbone amide ^{15}N resonances of proline were assigned with ct versions (Liu, 1999) of the 2D HA(CACO)N and 2D HA(CA)N experiments (Wang et al., 1995). The proline amide ^{15}N resonances in hPrP(23–230) could thus be assigned, with the exceptions of the prolines in the octapeptide repeats, which show extensive resonance overlap, and Pro 50 and Pro 51, which have degenerate $^1H^{\alpha}$, $^1H^{\delta}$ and ^{15}N resonances.

Survey of the resonance assignments obtained for the tail in hPrP(23–230)

A survey of the results obtained with the experiments of Figures 3 and 4 is provided in Figure 8. In addition to the data shown in Figures 5–7, the following assignments are particularly nice illustrations of the potentialities of the new experiments. The amide resonances of Gly 35, Gly 93, Gly 94 and Gly 124 are overlapped with those of Gly residues in the octapeptide repeats and could not have been assigned with conventional experiments. In 3D (H)N(CO-TOCSY)NH these resonances can be assigned from their connections with the preceding and succeeding residues, which have in all these cases resolved diagonal peaks. The Ala residues 116, 117 and 118 have different $^1H^N$ chemical shifts but their ^{15}N chemical shifts could only be distinguished in the 3D (H)N(CO-TOCSY)NH spectrum, where Ala 116 could be connected to Ala 115 and Ala 118 to Gly 119. With a 2D (H)N(CO-TOCSY-N)H spectrum the tripeptide segments Gly-Trp-Gly in the second, third and fourth octapeptide repeats could be distinguished from each other on the basis of the small $^1H^N$ chemical shift differences among the cross peaks linking the Trp residues with their flanking Gly residues, but they could not be assigned individually due to other resonance degeneracies involving also the proline residues. Individual assignments of the pentapeptide segments Gln-Pro-His-Gly-Gly in the second to fifth octapeptide repeats could not be achieved because of extensive resonance degeneracy. By using the 3D (H)CA(CO-TOCSY)NH and 3D (H)CBCA(CO-TOCSY)NH experiments, the sequential connectivities of the tail of hPrP(23–230) from Lys 23 to Gly 124 could otherwise be established, including five connectivities between residues that are separated in the sequence by prolines.

Side chain assignments in the tail of hPrP(23–230) were obtained with high resolution versions of (H)CC(CO)NH-TOCSY and H(CCCO)NH-TOCSY

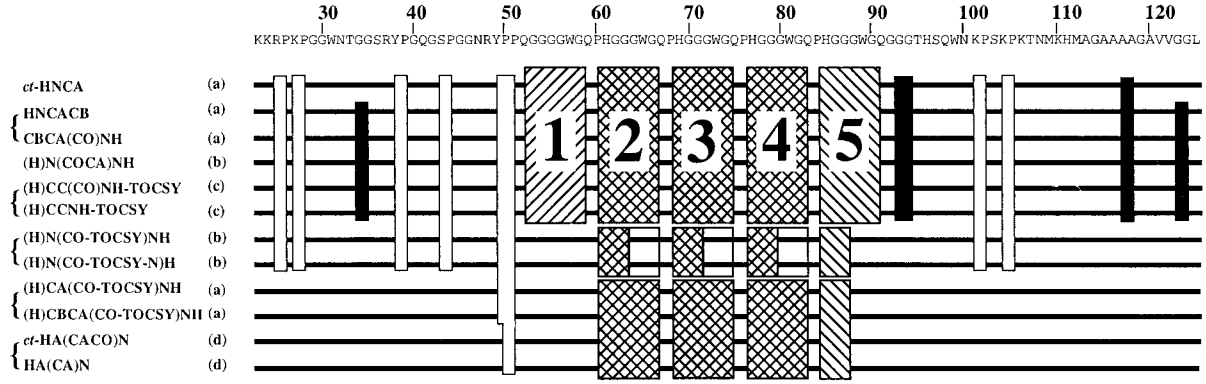

Figure 8. Survey of the sequential assignments obtained for the N-terminal tail of residues 23–125 of hPrP(23–230). Below the amino acid sequence the horizontal lines represent the backbone sequential connectivities established using the NMR experiments indicated on the left. The vertical empty boxes indicate missing cross peaks (including proline residues), and black boxes indicate resonance overlap. The shaded boxes numbered 1 to 5 represent part or all of the five octapeptide repeats, depending on the octapeptide repeat and the experiment. Inside these boxes no unambiguous sequential assignments could be established due to signal overlap. The lines (a) represent experiments that correlate $^{13}C^{\alpha}$ or $^{13}C^{\alpha/\beta}$ with the backbone amide moieties. The lines (b) represent experiments that give sequential amide-to-amide connectivities. The lines (c) represent experiments that correlate side-chain resonances with the corresponding backbone amide moieties. The lines (d) represent experiments that correlate $^{1}H\alpha$ with the backbone amide moieties. Experiments that were used in pairs to obtain sequential connectivities are linked with curly brackets.

experiments (Grzesiek et al., 1993a; Logan et al., 1993), using very long ct ^{15}N evolution times (400 ms) and band-selective $^{13}C^{\alpha}$ decoupling during the ^{15}N evolution period (Liu, 1999). A complete list of the assignments obtained has been deposited in the BioMagResBank, accession No. 4402. Supplementary material from the Ph.D. Thesis of A. Liu (1999) is available on our Web Page http://www.mol.biol.ethz.ch/wuthrich.

Conformation-dependent C^{α} chemical shifts

Based on relaxation data, the N-terminal tail of murine PrP(23–231) (Riek et al., 1997) and hPrP(23-230) (Zahn et al., 2000) is flexibly disordered. The C^{α} chemical shifts show deviations from the random coil values that are within ± 0.5 ppm, thus indicating that there are no sizeably populated standard secondary structure elements in the tail. A detailed interpretation of the chemical shifts, NOE data and relaxation times in the tail of prion proteins is in progress.

Acknowledgements

Financial support was obtained from the Schweizerischer Nationalfonds (project 438+.50287) and an exchange fellowship of the ETH Zürich to A.L. We are grateful to Drs. K. Pervushin and R. Wimmer for useful discussions.

References

Abragam, A. (1961) *Principles of Nuclear Magnetism*, Oxford University Press, New York, NY, pp. 305ff.
Bartels, Ch., Xia, T., Billeter, M., Güntert, P. and Wüthrich, K. (1995) *J. Biomol. NMR*, **6**, 1–10.
Bax, A. and Grzesiek, S. (1993) *Acc. Chem. Res.*, **26**, 131–138.
Bax, A. and Ikura, M. (1991) *J. Biomol. NMR*, **1**, 99–104.
Bodenhausen, G. and Ruben, D. (1980) *Chem. Phys. Lett.*, **69**, 185–188.
Bracken, C., Palmer III, A.G. and Cavanagh, J. (1997) *J. Biomol. NMR*, **9**, 94–100.
Braun, D., Wider, G. and Wüthrich, K. (1994) *J. Am. Chem. Soc.*, **116**, 8466–8469.
Braunschweiler, L. and Ernst, R.R. (1983) *J. Magn. Reson.*, **53**, 521–528.
Bundi, A. and Wüthrich, K. (1979) *Biopolymers*, **18**, 299–311.
Cavanagh, J., Palmer III, A.G., Wright, P.E. and Rance, M. (1991) *J. Magn. Reson.*, **91**, 429–436.
Donne, D.G., Viles, J.H., Groth, D., Mehlhorn, I., James, T.L., Cohen, F.E., Prusiner, S.B., Wright, P.E. and Dyson, H.J. (1997) *Proc. Natl. Acad. Sci. USA*, **94**, 13452–13457.
Dyson, H.J. and Wright, P.E. (1998) *Nat. Struct. Biol.*, **5**, 499–503.
Grzesiek, S. and Bax, A. (1992) *J. Am. Chem. Soc.*, **114**, 6291–6293.
Grzesiek, S. and Bax, A. (1993) *J. Am. Chem. Soc.*, **115**, 12593–12594.
Grzesiek, S. and Bax, A. (1997) *J. Biomol. NMR*, **9**, 207–211.
Grzesiek, S., Anglister, J. and Bax, A. (1993a) *J. Magn. Reson.*, **B101**, 114–119.
Grzesiek, S., Anglister, J., Ren, H. and Bax, A. (1993b) *J. Am. Chem. Soc.*, **115**, 4369–4370.
Güntert, P., Dötsch, V., Wider, G. and Wüthrich, K. (1992) *J. Biomol. NMR*, **2**, 619–629.
Kay, L.E., Keifer, P. and Saarinen, T. (1992) *J. Am. Chem. Soc.*, **114**, 10663–10665.

Kay, L.E., Ikura, M., Tschudin, R. and Bax, A. (1990) *J. Magn. Reson.*, **89**, 496–514.
Kupče, E. and Freeman, R. (1995) *J. Magn. Reson.*, **A115**, 273–276.
Liu, A. (1999) *NMR Spectroscopy with Prion Proteins and Prion Protein Fragments*, Ph.D. Thesis No. 13234, ETH Zürich.
Logan, T.M., Olejniczak, E.T., Xu, R.X. and Fesik, S.W. (1993) *J. Biomol. NMR*, **3**, 225–231.
Marion, D., Ikura, M., Tschudin, R. and Bax, A. (1989) *J. Magn. Reson.*, **85**, 393–399.
Matsuo, H., Kupce, E., Li, H. and Wagner, G. (1996) *J. Magn. Reson.*, **B111**, 194–198.
McCoy, M. and Mueller, L. (1992) *J. Am. Chem. Soc.*, **114**, 2108–2112.
McCoy, M. and Mueller, L. (1993) *J. Magn. Reson.*, **A101**, 122–130.
Morris, G.A. and Freeman, R. (1979) *J. Am. Chem. Soc.*, **101**, 760–762.
Muhandiram, D.R. and Kay, L.E. (1993) *J. Magn. Reson.*, **B103**, 203–216.
Rance, M. (1987) *J. Magn. Reson.*, **74**, 557–564.
Riek, R., Hornemann, S., Wider, G., Glockshuber, R. and Wüthrich, K. (1997) *FEBS Lett.*, **413**, 282–288.
Santoro, J. and King, G.C. (1992) *J. Magn. Reson.*, **97**, 202–207.
Schätzl, H.M., Da Costa, M., Taylor, L., Cohen, F.E. and Prusiner, S.B. (1995) *J. Mol. Biol.*, **245**, 362–374.
Shaka, A.J., Barker, P.B. and Freeman, R. (1985) *J. Magn. Reson.*, **64**, 547–552.
Shaka, A.J., Lee, C.J. and Pines, A. (1988) *J. Magn. Reson.*, **77**, 274–293.
Shaka, A.J., Keeler, J., Frenkiel, T. and Freeman, R. (1983) *J. Magn. Reson.*, **52**, 335–338.
Sørensen, O.W., Rance, M. and Ernst, R.R. (1984) *J. Magn. Reson.*, **56**, 527–534.
Tycko, R., Pines, A. and Gluckenheimer, R. (1985) *J. Chem. Phys.*, **83**, 2775–2802.
Vuister, G.W. and Bax, A. (1992) *J. Magn. Reson.*, **98**, 428–435.
Wang, A.C., Grzesiek, S., Tschudin, R., Lodi, P.J. and Bax, A. (1995) *J. Biomol. NMR*, **5**, 376–382.
Wider, G. (1998) *Prog. NMR Spectrosc.*, **32**, 193–275.
Wittekind, M. and Müller, L. (1993) *J. Magn. Reson.*, **B101**, 201–205.
Wüthrich, K. (1986) *NMR of Proteins and Nucleic Acids*, Wiley, New York, NY.
Wüthrich, K. (1994) *Curr. Opin. Struct. Biol.*, **4**, 93–99.
Zahn, R., von Schroetter, C. and Wüthrich, K. (1997) *FEBS Lett.*, **417**, 400–404.
Zahn, R., Liu, A., Lührs, T., Riek, R., von Schrötter, C., Lopez-Garcia, F., Billeter, M., Calzolai, L., Wider, G. and Wüthrich, K. (2000) *Proc. Natl. Acad. Sci. USA*, **97**, 145–150.